RADIONUCLIDE IMAGING

INTRODUCTION

Radionuclide imaging is performed in nuclear medicine clinics and positron emission tomography (*PET*) centers. In both cases, radionuclides are used to label interesting compounds (radiopharmaceuticals) that are injected into patients. The distribution and kinetics of these radiotracers reveal the physiology of tissues and organs and thereby provide diagnostic information. Radionuclides are nearly ideal as tracers. Although they can be readily detected outside the body, the total mass of the radionuclides administered for diagnostic studies is typically in the nanogram range. Thus, the toxic and perturbing effects of the radionuclides are minimal. Radiotracers used in conventional nuclear medicine studies are imaged with a scintillation camera. The scintillation camera is used for imaging conventional planar (2-D) studies and single photon emission computed tomography studies (*SPECT*). PET systems image the annihilation radiation resulting from positron emitting radionuclides using coincidence detection. This article will review the principles of these radionuclide imaging systems. It will begin with a brief summary of radioactive decay and the interactions of γ rays with materials. Radiation detection and imaging devices will be discussed next. The factors that degrade radionuclide images will be reviewed along with techniques to improve image quality. The article will be concluded with a discussion of clinical nuclear medicine and PET applications of radionuclide imaging along with pre-clinical small animal imaging systems.

RADIOACTIVE DECAY

Energy Units

In atomic and nuclear physics, energy is typically expressed in units of electron volts. One electron volt is equal to the kinetic energy of an electron accelerated through a 1-volt potential. Visible light has photon energy of 2–3 eV. The energy of γ rays is much higher and is usually given in terms of keV (1 keV = 1000 eV) or MeV (1 MeV = 1,000,000 eV). The masses of atomic and nuclear particles are also commonly expressed in units of MeV calculated from the Einstein equation ($E = mc^2$).

Nuclear Nomenclature

Radioactive decay has a nuclear origin. Although the nucleus occupies a very small fraction of the volume of an atom, it has virtually all the mass. The nucleus consists of A nucleons (Z protons and N neutrons), held together by the strong force. Different nuclear species are referred to as nuclides and they are represented by ${}^{A}X$, where X is the chemical symbol associated with the nuclide. Nuclides with the same Z and different N are called isotopes, whereas those with the same N are called isotones. Nuclides with the same A are called isobars. Nucleons have discrete energy levels, and when a nucleon is in an excited state, it returns to the ground state with the emission of a high energy photon called a γ ray.

Some nuclides such as ${}^{16}O$ never change their nuclear identity and are said to be stable. Others, such as ${}^{14}C$, spontaneously change into another nuclide with the emission of energetic particles. These nuclides are called radioactive. Three primary types of radioactive emissions exist: α particles, β particles, and γ radiation. α particles are helium nuclei that are emitted through a quantum mechanical tunneling process, and as no α emitters are used in radionuclide imaging, they will not be discussed further. β particles are high energy electrons or positrons that are created as part of an isobaric decay process in which one nucleon is transformed into its counterpart. There are three modes of β decay, $\beta-$, $\beta+$, and EC (*EC*); these modes will be discussed in more detail below.

α and β particles have short ranges in tissue (< 0.1 millimeters for α and < 10 millimeters for β). Thus, they deliver a radiation dose to the patient without yielding useful information. γ rays, however, are very penetrating and can be detected externally. Radionuclides that emit γ rays without emitting any charged particles are especially attractive as imaging tracers because they deliver a low radiation dose to the body. Table 1 has a list of γ emitting radionuclides along with their physical properties.

γ rays, as noted above, are high energy, monoenergetic photons resulting from the transition of a nucleon from an excited state to a lower energy level. This process is called an isomeric transition (*IT*). In some nuclides, only one transition occurs from the excited state to the ground state and only a single γ ray is emitted. In other nuclides, intermediate states exist, so more than 1 γ ray may be emitted. Quite often (not always) α or β emission will leave the daughter nuclide in an excited state so that γ radiation frequently accompanies the other decay modes. In most cases, the emission of the γ ray is virtually instantaneous ($< 10^{-24}$ sec). For some nuclides, the excited state persists for seconds, hours, or even days. These states are called isomeric or metastable states and they are denoted with an "m" following the atomic mass number. Technetium-99m (${}^{99m}Tc$) is an extremely important example of a metastable radionuclide in radionuclide imaging.

β Decay

β decay is a manifestation of the weak force in which nucleon exchange occurs. Either a proton is changed into a neutron or a neutron is changed into proton. The atomic mass remains constant and the atomic number changes by either +1 or −1. $\beta-$ decay occurs in unstable nuclides that have a relative abundance of neutrons. With $\beta-$ decay, a neutron is changed into a proton and the Z of the daughter nuclide is increased by 1. During the process of $\beta-$ decay, an energetic electron is created and emitted along with a massless, neutral particle, the anti-neutrino. $\beta-$ radionuclides are produced from neutron activation of stable nuclides or are separated from fission byproducts in a nuclear reactor. As a result of the β particle, $\beta-$ emitters are not preferred for imaging studies, but are sometimes used because no suitable alternatives exist. ${}^{133}Xe$ and ${}^{131}I$ are examples of $\beta-$ emitters that are used for imaging.

Table 1. Radionuclides Commonly Used in Medical Imaging

Radionuclide	Decay Mode	Production Method	Half Life	Principal Photon Emissions (keV)
^{99m}Tc	IT	^{99}Mo Generator	6 hr	140
^{81m}Kr	IT	^{81}Rb Generator	13 sec	190
^{133}Xe	β-	Fission Byproduct	5.3 dy	30, 80
^{131}I	β-	Fission Byproduct	8 dy	364
^{111}In	EC	^{111}Cd(p, n)^{111}In	67 hr	172, 247
^{67}Ga	EC	^{68}Zn($p, 2n$)^{67}Ga	78 hr	93, 185, 296
^{123}I	EC	^{124}Te($p, 5n$)^{123}I	13 hr	159
^{201}TI	EC	^{201}Hg($d, 2n$)^{201}TI	73 hr	60–80 (X rays), 167
^{15}O	β+	^{14}N(d, n)^{15}O	122 sec	511
^{13}N	β+	^{16}O(p, α)^{13}N	10 min	511
^{11}C	β+	^{10}B(d, n)^{11}C	20 min	511
^{18}F	β+	^{18}O(p, n)^{18}F	110 min	511
^{82}Rb	β+	^{82}Sr Generator	75 sec	511

Table 2. Scintillation Properties of NaI(TI), BGO, LSO, and GSO

Properties	NaI(TI)	BGO	LSO	GSO
Effective Z	50	74	66	60
Density	3.67	7.13	7.4	6.71
μ (cm^{-1}) @ 511 keV	0.33	0.91	0.833	0.684
Max Emission λ (nm)	410	480	420	430
Relative light output	1	0.1	0.75	0.35
Decay time (nsec)	230	300	40	60
Refractive index	1.85	2.15	1.82	1.85

Table 3. Nuclear Medicine and PET Diagnostic Studies

Radiopharmaceutical	Application
^{99m}Tc Medronate (MDP), Oxidronate (HDP)	Bone scans
^{99m}Tc Sestamibi, Tetrofosmin	Myocardial perfusion, breast cancer
^{99m}Tc Pentetate (DTPA)	Renal function (GFR)
^{99m}Tc Mirtiatide (MAG3)	Renal function (Flow)
^{99m}Tc Macroaggregated Albumin (MAA)	Lung perfusion
^{99m}Tc Red Blood Cells	Cardiac wall motion, LV Ejection fraction
^{99m}Tc Exametazine (HMPAO), Bicisate (ECD)	Brain perfusion
^{99m}Tc Desofenin (DISIDA), Lidofenin (HIDA), Mebrofenin	Hepatobilliary function
^{99m}Tc Arcitumomab (CEA Scan)	Colon cancer
^{133}Xe	Lung ventilation, cerebral blood flow
^{131}I Metaiodobenzylguanidine (MIBG)	Neuroendocrine tumors
^{131}I Sodium Iodide	Thyroid cancer
^{67}Ga Citrate	Infection, tumor localization
^{111}In Oxine	Leukocyte & platelet labeling (Infection)
^{111}In Capromab Pendetide (ProstaScint)	Prostate cancer
^{111}In Pentetreotide (OctreoScan)	Neuroendocrine cancer
^{201}TI Thallous Chloride	Myocardial perfusion
^{123}I Sodium Iodide	Thyroid cancer
^{15}O Water	Regional cerebral blood flow
^{13}N Ammonia	Myocardial perfusion
^{11}C Acetate	Myocardial function
^{11}C Methionine	Tumor localization
^{18}F Fluoro-2-deoxyglucose (FDG)	Tumor localization, myocardial viability seizure localization
^{18}F Fluro-Labeled Thymidine (FLT)	Tumor proliferation
^{82}Rb	Myocardial perfusion

The other two modes of β decay, β+ and EC decay, occur for nuclides with an abundance of protons. In both of these modes, a proton is changed into a neutron and the Z of the daughter nuclide is decreased by 1. In EC, an inner shell orbital electron is captured in the nucleus and is used in the conversion of a proton into a neutron. During this process, a neutrino is created, but no charged particles are emitted, and this feature makes them attractive as imaging agents. There will be characteristic X rays and Auger electrons emitted as the electron vacancy is filled, and sometimes the characteristic X rays are collected along with the γ rays to form images. EC radionuclides are pro-

duced in charged particle accelerators such as a cyclotron (1). ^{201}TI, ^{123}I, ^{111}In, and ^{67}Ga are examples of commonly used EC radionuclides.

β+ decay results in the emission of a positron as a proton is changed into a neutron. A positron is the anti-particle of the electron having the same mass and other quantum properties of the electron, but has a positive charge. The energetic positron dissipates its energy within a few millimeters and captures an electron. Within a very short time, the positron and electron mutually annihilate each other, yielding two co-linear 511-keV photons. The coincidence detection of these two photons provides the basis of PET imaging. Charged particle accelerators, typically cyclotrons, produce positron emitters (1, 2). Some of the positron emitters that are useful for medical imaging, such as ^{11}C, ^{13}N, and ^{15}O, have short half lives that require an on-site accelerator. Fluorine-18 (^{18}F) with a 110-minute half life can be shipped over short distances and is commercially available.

Radioactivity

Radioactivity is a measure of the number of decays per second in a sample and is defined by the equation

$$A = \lambda N \tag{1}$$

where A is the activity (decays per second), N is the number of radioactive atoms, and λ is the decay constant (defined below). The former unit of radioactive decay was the Curie, 3.7×10^{10} decays per second, while the SI unit for radioactive decay is the becquerel (Bq), 1 decay/second. Typically, 1 to 30 mCi (~40 MBq to 1000 MBq) are administered for diagnostic imaging studies depending on the radionuclide. Although radioactive decay occurs at random, the probability of decay over a fixed time interval (the decay constant, λ) is constant and unique for every radionuclide. The decay of a radioactive source is an exponential function:

$$A(t) = A_0 \exp(-\lambda t) \tag{2}$$

$$N(t) = N_0 \exp(-\lambda t) \tag{3}$$

where A_0 is the initial quantity of activity, No is the initial number of radioactive atoms, and $A(t)$ and $N(t)$ are the quantities at some later time t. Because the fractional decrease over any fixed time interval remains constant, one can use the half-life ($T_{1/2}$) to characterize the decay behavior. The half-life is the time interval in which the activity (or number of radioactive atoms) decreases by a factor of two. The relationship between the half-life and the decay constant is:

$$\mathrm{T}_{1/2} = \ln(2)/\lambda = 0.693/\lambda \tag{4}$$

The half lives for radionuclides used in radionuclide imaging range from seconds (e.g., ^{81m}Kr $T_{1/2} = 13$ s) to days (^{131}I $T_{1/2} = 8$ days).

COUNTING STATISTICS

The emission and detection of γ rays is governed by Poisson statistics. As a result, the uncertainty (standard deviation) of a measurement with N counts is $N^{1/2}$. If precision is defined as $100\% \times N^{1/2}/N$, then it is obvious that precision improves (gets smaller) as N increases (Fig. 1). Subtle details in images are often lost in the statistical fluctuations (image noise). Therefore, it is desirable to acquire as many detected events as possible to maintain good image quality. As the detection efficiency for γ rays in imaging systems is low, this requirement often presents a problem because limitations exist both on the amount of radioactivity that can be administered to a patient and on the study duration. Arithmetic operations on radionuclide images propagate the individual uncertainties into the result. For example, when images are subtracted, areas where the result is close to zero will be especially noisy. Image noise is also a major limiting factor in SPECT and PET imaging, as the reconstruction algorithm both amplifies and spatially correlates the image noise.

γ RAY INTERACTIONS WITH THE MATTER

The intensity of a γ-ray beam decreases as it traverses through a material because of interactions between the γ rays and the electrons in the material. This process is referred to as attenuation. Attenuation is an exponential process described by

$$I(x) = I_0 \exp(-\mu x) \tag{5}$$

where I_0 is the initial photon intensity, $I(x)$ is the photon intensity after traveling a distance x through the material, and μ is the linear attenuation coefficient of the material. Over the range of γ-ray energies used in radionuclide imaging, the two primary interactions that contribute to the attenuation coefficient are photoelectric absorption and Compton scattering.

Photoelectric absorption refers to the total absorption of the γ ray by an inner shell atomic electron. The inner shell electron is ejected from the atom with an energy equal to the γ-ray energy—the binding energy of the electron. Photoelectric absorption can only occur with electrons whose binding energy is less than the γ-ray energy. The cross section for photoelectric absorption (τ) is proportional to the media density, the cube of the atomic number and is inverse the proportional to the cube of the γ-ray energy ($\tau \propto \rho Z^3/E\gamma^3$). As a result of the low effective Z of body tissues ($Z_{\mathrm{eff}} = 7.6$), photoelectric absorption is not the dominant interaction. However, it is the primary interaction in high Z detecting materials such as sodium iodide, bismuth germanate, and shielding material such as lead, which is advantageous, because the signal generated by photoelectric absorption is proportional to the total γ-ray energy.

Compton scattering occurs when the incoming γ ray interacts with a loosely bound outer shell electron. A portion of the γ-ray energy is imparted to the electron and the remaining energy is left with the scattered photon. The amount of energy lost in the scattering event depends on the angle between the incident γ ray and scattered photon. The cross section for Compton scattering (σ) depends on the electron density of the media and is (approximately) inversely proportional to the γ-ray energy ($\sigma \sim \rho_e/E_\gamma$). Compton scattering is the dominant interaction in body tissues,

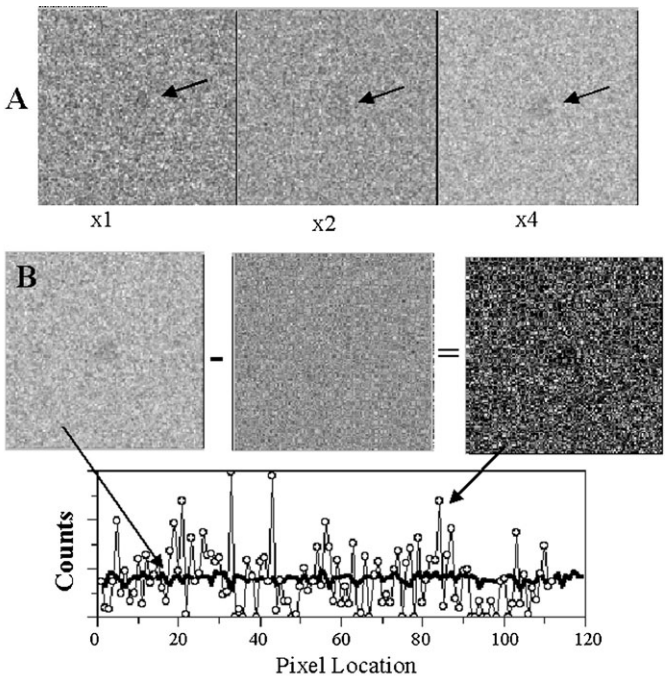

Figure 1. Image noise. The detection and emission of radiation is governed by Poisson statistics. As a result, the precision of a count measurement improves as the number of detected counts increase. Figure 1(**a**) shows a series of four images of a circular defect with a 5% defect. Each succeeding image to the right has a factor of two increase in the count density. Note that as the count density increases, the relative level of the noise decreases and the defect becomes more perceptible. Figure 1(**b**) illustrates how statistical errors propagate with arithmetic operations. The resulting subtracted image has a mean near zero with a standard deviation that is larger than either of the original images. The graph below the images shows a count profile through the image labeled B along with a profile through the result of the subtraction.

and it contributes significantly to the attenuation of 511-keV photons in the shielding and detecting materials.

SCINTILLATORS

The efficient detection of γ rays requires detectors with high density, high atomic number, and a large sensitive volume. Scintillators are the most common type of detector used in radionuclide imaging (3). Scintillators emit a flash of visible light photons when they absorb γ rays. The brightness of the scintillation is directly proportional to the absorbed energy of the detected event. Although a large number of scintillators are used in medical applications, the most common in single photon imaging is sodium iodide activated with thalium (NaI(Tl)), whereas the scintillators used in PET imaging include bismuth germanate (*BGO*), gadolinium oxyorthosilicate (*GSO*), and lutetium oxyorthosilicate (*LSO*). Table 2 lists the physical properties of these detectors.

Although it is expected that scintillators will remain the preferred detectors in PET, applications exist within conventional radionuclide imaging where semiconductor detectors are making inroads. Both cadmium telluride-and cadmium zinc telluride-based γ imaging systems are currently available for imaging low energy γ-ray emitters such as ^{99m}Tc (4).

Electronics

All scintillation detectors (individual detectors and imaging devices) use similar electronics as shown in Fig. 2. In discrete detectors, the scintillation is converted to an electronic pulse by a photomultiplier tube, although solid-state devices such as avalanche photodiodes are beginning to replace these devices (5). The pulse is further amplified and shaped and is sampled by a pulse height analyzer. The pulse height analyzer identifies pulses of a pre-selected amplitude range corresponding to the desired γ-ray energy. Pulses falling within this range trigger a standard signal that is counted by a scaler or other counting device. All other pulses are ignored. As the pulse height maintains its proportional relationship with the energy absorbed in the scintillator, the pulse height analyzer can be calibrated in keV units.

Intrinsic efficiency

The intrinsic efficiency of a detector (denoted by ε) is determined by its thickness (x) and its linear attenuation coefficient (μ):

$$\varepsilon = 1 - \exp(-\mu x) \tag{6}$$

The intrinsic efficiency is high (i.e., close to 1) when the product μx is large, which requires that μ or x or both are large. Increasing the detector thickness adversely affects spatial resolution from parallax errors, so it is preferable to have a large μ. Detector materials with high density

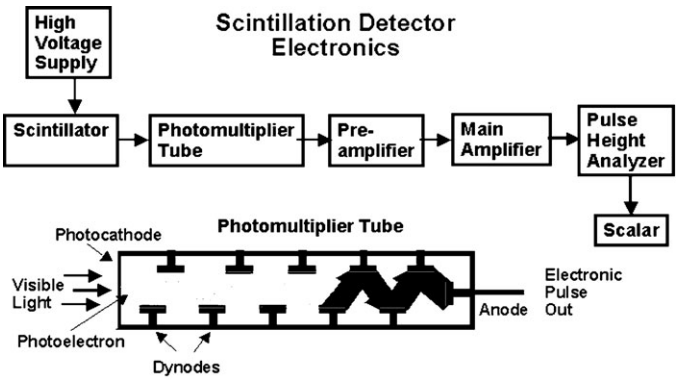

Figure 2. Scintillation detector electronics. The components in scintillation detectors are similar. The detector is optically coupled to a photomultiplier tube that converts the scintillation into an electronic pulse. The visible light generates photoelectrons at the photocathode. These electrons are accelerated to a terminal post called a dynode with sufficient energy (usually about 100 eV) to free four to five new electrons, which continues through a succession of dynodes to achieve an overall signal gain of >1,000,000. The output of the photomultiplier tube gets a power boost from the pre-amplifier and is transmitted to the main amplifier where the signal is shaped and amplified. At this point, it is sent to the pulse height analyzer. If the pulse amplitude lies between the upper and lower thresholds (energy window), a logic pulse is generated indicating a good event. The scale counts and records the number of good events.

and high atomic number are especially important for coincidence detection of the 511-keV annihilation radiation. As both photons have to be detected to register a valid coincidence event, the coincidence detection efficiency is ε^2.

Energy Resolution

As γ rays are monoenergetic, a detector with perfect energy resolution would generate pulses with the same amplitude for each γ ray that was totally absorbed. The energy spectrum for such a device would be a delta function. Scintillation detectors do not have perfect energy resolution because of statistical fluctuations in the number of electrons liberated at the photocathode of the photomultiplier tube. The noise level associated with these electrons is decreased as the brightness of the scintillation increases. As a result, the efficient conversion of absorbed γ-ray energy into visible light is an important feature. Both NaI(Tl) and LSO have high light outputs, while BGO is an order of magnitude lower. In addition, their refractive index is better matched to the glass face of the photocathode. Energy resolution is quantified from the width of the energy peak measured in keV at the half maximum level (full-width-at-half maximum, FWHM):

$$\text{Energy Resolution} = 100\% \times \text{FWHM(keV)}/E\gamma\text{(keV)} \quad (7)$$

Good energy resolution is important for rejecting scattered radiation, a major factor in reducing image contrast. If a γ ray is Compton scattered within the patient, it necessarily loses energy. When the energy resolution is good, a narrow energy window can be set on the photopeak restricting the number of scattered photons. With poor energy resolution, a broad window has to be used to maintain sensitivity, and more scattered radiation is included in the acquired image data.

The energy resolution of NaI(Tl) is sufficient to permit the simultaneous acquisition information from γ rays of different energy, which is accomplished by selecting individual energy windows on multiple pulse height analyzers for each of the desired γ rays. In the single isotope mode, the information from all of the selected energy windows is summed and stored as one image. Studies using radionuclides with multiple γ-ray emissions like ^{111}In (172, 247 keV) or ^{67}Ga (93, 185, 300 keV) are examples. In the multiple isotope mode, separate images are generated for each selected energy window, which yields spatially registered images with unique information. One application of dual isotope imaging is ^{99m}Tc MDP bone scanning in conjunction with ^{111}In white cell labeling for localizing sites of infection. In PET imaging, this type of acquisition has been used to simultaneously collect a coincidence emission study and a single photon transmission study with ^{137}Cs($E\gamma$ = 662 keV) for attenuation correction.

Temporal Resolution

It is important to realize that every event detected by a radionuclide imaging device is analyzed individually. As the conversion of γ-ray energy into an electronic pulse is not instantaneous, the detection process requires a finite amount of time. If an additional event occurs before the system has finished processing the previous one, pulse information is compromised and the events cannot be properly interpreted. The length of time it takes to process an event is often called the dead time, because the system appears to be insensitive during this time. The primary limiting factor in scintillation detectors is the length of time the scintillation persists. Both NaI(Tl) and BGO are relatively slow scintillators, whereas LSO and GSO are 6–7 times faster. Fast scintillators have an additional benefit for PET because they allow a narrower coincidence time window thus reducing the level of accidental coincidences. They also provide the potential for time-of-flight PET imaging discussed below.

Few single photon studies exist that are limited by the count rate capability of NaI(Tl) because of the very low count sensitivity of the collimator. However, the ability to handle high count rates is crucial for PET systems, where the unshielded detectors often achieve singles counting rates in the range where count rate losses are apparent

(6).

Scintillation Camera

Conventional nuclear medicine images are acquired on scintillation cameras (also referred to as Anger or γ cameras). The detector of the scintillation camera is a large ($\sim$50 $\times$ 40 cm), thin (9 mm) NaI(Tl) crystal (Fig. 3). The location of a γ-ray interaction is determined by the position-weighted average of the electronic pulses generated by the photomultiplier tubes in the vicinity of the absorption. Photomultiplier tubes are arranged in a close-packed array covering the entire sensitive area of the crystal. In addition to estimating the position of the scintillation event, the photomultiplier tube signals are also combined to estimate the energy absorbed in the interaction. The energy signal is used to discriminate against scattered radiation and is also used to normalize the position signals so that the size of the image does not depend on the γ-ray energy.

As the sampling and response of the photomultiplier tubes to individual scintillations is not uniform, additional corrections are made for position-dependent shifts in the energy signal (referred to as Z or energy correction) and in the determination of the event location (referred to as L or spatial linearity correction). Thus, when a γ ray is absorbed, the scintillation camera must determine the position and energy of the event, determine if the energy signal falls within a selected pulse height analyzer window, and apply spatial linearity correction. At this point, the location corresponding to the event within a pre-selected image matrix is incremented. A scintillation camera image is generated from the accumulation of these events.

γ rays cannot be focused because of their high photon energy. Therefore, a collimator must be used to project the distribution of radioactivity within the patient onto the sodium iodide crystal. A collimator is a multi-hole lead device that selectively absorbs all γ rays except those that traverse the holes, which severely restricts the number of emitted γ rays that can be detected. Less than 0.05% of the γ rays that hit the front surface of the collimator are transmitted through to the crystal. Most collimators have a parallel hole design, although diverging, converging (cone beam), and fan beam geometries are available. As the design parameters that favor good spatial resolution (small hole size and extended length) adversely affect the collimator sensitivity, collimators are optimized for the type of imaging required. The energy of the γ rays being imaged is also a factor in the design of a collimator, as high energy photons require thicker septa between the holes. Thus, medium energy collimators (designed for $E_\gamma > 200$ keV) and high energy collimators (designed for $E_\gamma > 350$ keV) have lower sensitivity and poorer spatial resolution than those designed for the 140-keV γ rays from ^{99m}Tc.

EMISSION TOMOGRAPHY

Two kinds of emission tomographic imaging systems exist: single photon emission computed tomography (*SPECT*) and positron emission tomography (*PET*). SPECT systems use scintillation cameras to collect (attenuated) projection information, whereas PET systems use coincidence detection.

SPECT Systems

A SPECT system consists of one or more scintillation cameras mounted to a gantry that can revolve about a fixed axis in space, the axis of rotation (Fig. 4) (7). As projection views must be acquired from 360 degrees about the patient, additional scintillation cameras increase the sensitivity. The most common configuration available today is the dual detector system, which not only yields better SPECT sensitivity, it also allows the simultaneous acquisition of anterior and posterior views for conventional planar imaging. In the dual detector SPECT systems, each scintillation camera has the ability to move independently in the radial direction as the heads revolve about the patient, which allows body contouring and improves the overall spatial resolution of the study. SPECT systems are usually operated in a step-and-shoot mode. That is, the camera rotates over an angular increment and then remains motionless as it acquires a projection view. Alternatively, it is possible to acquire SPECT studies in a continuous rotation mode. In this mode, information is acquired into a pre-selected number of frames during the time the camera is a rotating continuously about the patient, each frame representing data acquired over a small, fixed angle of rotation.

Typically, 60–120 projection views are acquired over 360 degrees, which helps to partially compensate for attenuation. One exception is the myocardial perfusion study. As the heart is not centrally located in the thorax, most clinics acquire only the 180 degrees in which the heart is attenuated by the least amount of tissue. Although it causes some distortion, it yields tomographic images with higher contrast than those for which projections were acquired over the full revolution. To obtain accurate reconstructed images, corrections must be made for attenuation. An accurate correction for attenuation requires an estimate of the regional attenuation coefficients (attenuation map). Many SPECT systems use the Chang method, which presumes that the body is a uniform, unit density elliptical cylinder. A correction matrix is generated of the average attenuation factors for each point in the transverse plane. This correction matrix is then applied to the reconstructed image. Although this method works reasonably well in the abdomen and head, it is not effective in the thorax where most of the assumptions are invalid. SPECT systems can be equipped with a radionuclide transmission system that directly measures the attenuation map of the patient. An iterative reconstruction algorithm incorporates this information resulting in an accurate attenuation correction (8, 9). More recently, CT systems have been combined with SPECT systems to provide high quality anatomic information and even more accurate attenuation correction (10). Pictures of SPECT CT systems along with a clinical image are shown in Fig. 5.

PET Systems

Coincidence detection is used to detect the 511-keV photons resulting from positron annihilation (Fig. 6). As these photons are co-linear, one can determine the line along which the source is located from the simultaneous detec-

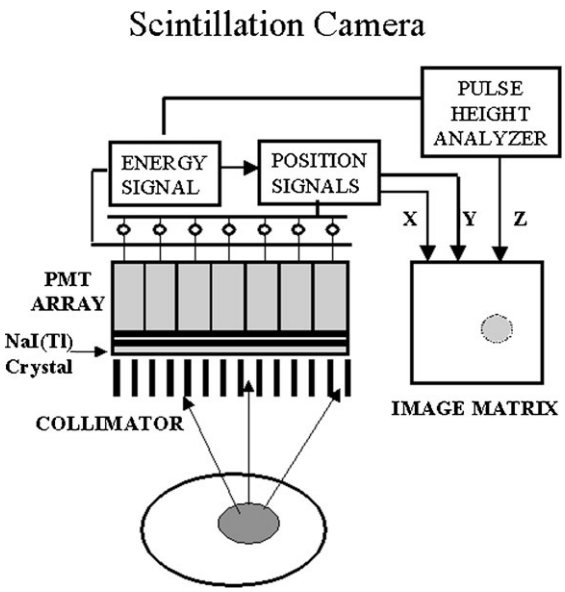

Figure 3. Scintillation camera. The scintillation camera uses one large, thin NaI(Tl) crystal as the sensitive element. γ or X rays from the internally distributed source are projected onto the NaI(Tl) crystal by the collimator, the image forming aperture of the scintillation camera. The scintillation resulting from γ-ray absorptions are sampled by photomultiplier tubes arranged in a close-packed array over the entire crystal surface. Location information is obtained from a position-weighted sum of the photomultiplier tube signals in the immediate vicinity of the interaction and energy information is obtained from the unweighted sum. The energy signal is used to normalize the position signals and to discriminate against scattered radiation. An event that meets the energy criteria is corrected for spatial linearity and uniformity, and it is registered by incrementing the pixel in a digital image corresponding to the event location on the crystal.

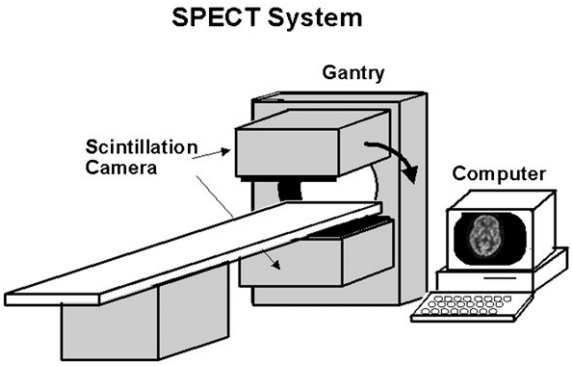

Figure 4. SPECT system. A SPECT system uses scintillation cameras to collect projection data. The scintillation cameras rotate about the patient collecting 60–120 views over a 360-degree rotation.

tion in opposing detectors. For a coincidence event to be registered, it must be detected by both detectors. Thus, if the detection efficiency for absorbing one of the annihilation photons is 0.30, then the coincidence efficiency is $0.3 \times 0.3 = 0.09$, which illustrates why high detection efficiency is critical. The time that it takes the detector to register an event is also very important. The decay time of the scintillation limits the ability of the system to accurately determine the timing of the associated electronic pulse. The coincidence time window used in PET imaging systems is on the order of 10 nanoseconds.

It is inevitable that the coincidence detectors will sometimes detect two unrelated events within the time window. These events are referred to as accidental or random coincidences. The random coincidence rate, C_R, depends on the size of the coincidence time window (Δt) and on the magnitude of the count rates at the two detectors (C_1, C_2).

$$C_R = 2 \times C_1 \times C_2 \times \Delta t \tag{8}$$

As random coincidences present unwanted background, it is important to keep this rate as low as possible. One way of accomplishing this feat is to restrict or shield against sources that are outside the coincidence field of view of the two detectors.

A PET imaging system consists of a large number of individual coincidence detectors (or multiple scintillation cameras) in coincidence (2, 7). The coincidence lines of response generate (attenuated) projection information without the need for collimation. As a result, the efficiency for detecting the 511-keV annihilation radiation is significantly higher than the efficiency for detecting low energy γ rays using collimators. Most dedicated PET systems use many individual detectors grouped in rings. Each detec-

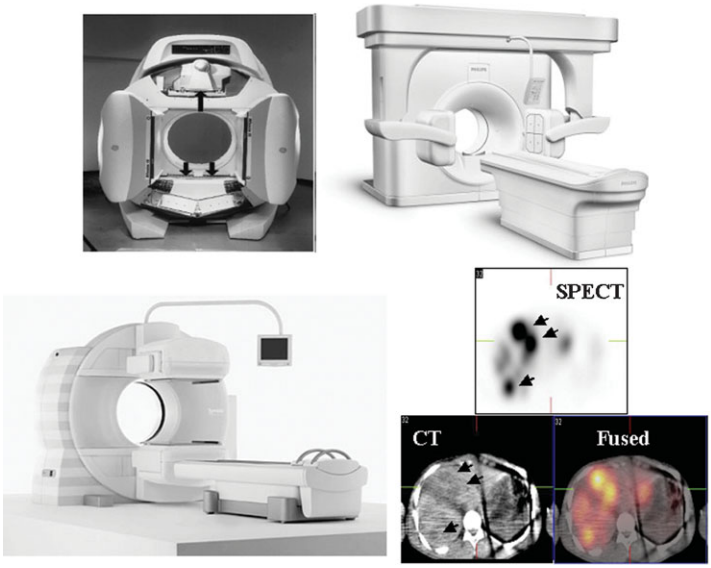

Figure 5. Commercial SPECT CT systems. These systems combine a CT system for anatomical information with a SPECT system. The devices shown are the GE Infinia Hawkeye, Philips Precedence, and Siemens Symbia. The lower right image shows an example of an ^{111}In Pentetreotide study in a patient with carcinoid along with co-registered CT images.

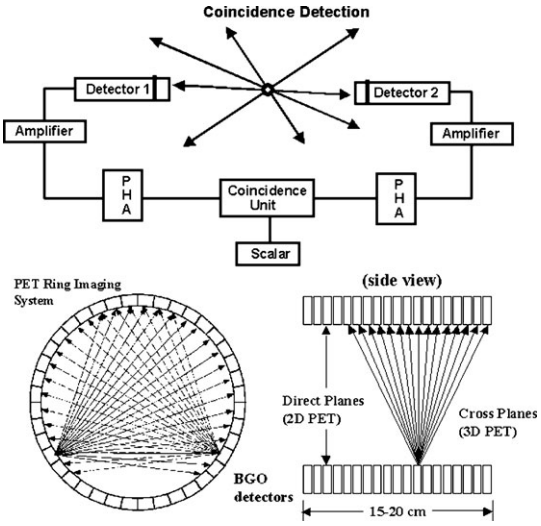

Figure 6. PET imaging system. PET imaging systems rely on the coincidence detection of the positron annihilation radiation. Opposed detectors register events that occur during a 10-nanosecond timing window. Although some PET tomographs use scintillation camera technology, most are made of a large number of individual coincidence detectors. For both designs, the lines of response are determined by the coincidence rays. Designs using individual detectors are arranged in rings. Multiple rings are stacked together to increase the axial field of view. PET cameras can be operated in the 2-D mode where only coincidence events in the plane of the ring or its adjacent neighbors are considered, or in the 3-D mode where are all coincidence paths are used.

tor forms a potential coincidence pair with the detectors on the opposite side of the ring, which provides sufficient sampling for generating tomographic images.

The acquired PET studies need several corrections, including corrections for the random coincidences, scatter, and attenuation. The random coincidence rate can be estimated using equation (9) if the individual count rates at each of the detectors are known. Scattered radiation cannot be totally eliminated by energy discrimination. Thus, estimates of scatter and a means for eliminating it are necessary. Corrections for attenuation require an estimate of the attenuation map for each reconstructed slice, which is typically measured on the PET system with the acquisition of a transmission study. It should be noted that the correction for attenuation in PET studies is large with maximum correction factors often greater than 100.

Pet imaging systems may be operated in the 2-D or 3-D modes. In the 2-D mode, the axial angle for coincidences is restricted to direct planes and the adjacent cross planes with lead shields, which reduces count sensitivity, but also reduces the magnitude of the scatter and random coincidence correction. The 3-D mode allows coincidence events

to be recorded over the entire axial field of view, which provides higher sensitivity and continuous axial sampling but with a significantly higher scatter fraction. 3-D PET also requires a 3-D reconstruction algorithm, which is computationally intensive and time-consuming. A more efficient approach re-bins the acquired data into appropriate 2-D data sets where conventional reconstruction algorithms can be applied (11, 12).

Recent developments in PET imaging include PET/CT hybrid imaging systems, the rebirth of time-of-flight PET, and small animal PET systems. Combined PET and CT imaging systems were introduced in 2000 and were rapidly embraced by the medical imaging community to the point that, within 2 years, they dominated the market. These devices consist of a high performance PET tomograph coupled to a high performance CT system sharing a common imaging table. Patients first get a helical CT study and then a PET study of the selected body region. The information from the CT scan is used to generate the attenuation correction factors required for the PET study and also provides high resolution anatomical images that are readily co-registered to the functional PET images (Fig. 7). These capabilities are particularly advantageous for oncology studies and account for the incredibly rapid growth of these devices in the medical community (13–15).

With conventional PET systems, the timing of coincident events is not precise enough to provide source localization. Light travels about 30 cm per nanosecond, and a time window of even several nanoseconds is too coarse to provide useful information. In the mid 1980s there was a PET tomograph based on barium fluorite (BaF_2) detectors that had very fast timing and could operate in the time-of-flight mode. However, the detection efficiency of BaF_2 was very poor and this device could not complete with conventional PET tomographs. Recently, a commercial time-of-flight PET system based on LYSO detectors has become available (13). This system has the capability of determining the source location to within several centimeters based on the time differential between the detection of the annihilation photons at two detectors. When this information is employed in the reconstruction algorithm, it improves the signal-to-noise-ratio, especially in large patients. This improvement in image quality can be used to reduce imaging time.

Reconstruction

Conventional nuclear medicine images are acquired with a scintillation camera positioned over the organ of interest. The resulting image is a 2-D *attenuated* projection of the 3-D distribution of radioactivity, and as a result, these images frequently suffer from low contrast. With the advent of computerized tomography in the mid-1970s, it became apparent that the same algorithms could be extended to emission imaging. Tomographic images of the internal distribution of a radiopharmaceutical can be reconstructed if a complete set of true projections is acquired. True projections are obtained from the line integrals of the radioactive distribution along a set of view angles. As a result of attenuation within the body, it is not possible to directly measure projection data. The techniques of tomographic reconstruction can still be applied, but unless corrections are made, there will be artifacts.

Although the detection mechanisms used by SPECT and PET are different, the steps for generating tomographic images are similar. Projections of the radioactivity distribution within the patient are acquired from a large number of views. These projections are organized by projection angle (sinogram) and, after the appropriate filter is applied, a computer algorithm is used to reconstruct the tomographic images. Two general reconstruction approaches exist: filtered backprojection and iterative reconstruction. With filtered backprojection, the projections are first modified by a windowed ramp filter and then backprojected at the angle at which they were acquired. Filtered backprojection has the advantage of being fast and easy to implement, but it cannot easily incorporate complex corrections.

The other approach to image reconstruction uses iterative algorithms (16). Iterative algorithms for image reconstruction were introduced in the 1970s with the introduction of X-ray computed tomography. These algorithms were extensions of general approaches to solving linear systems with sparse matrices. Figure 8 illustrates the method. An initial guess (usually a constant field) is used as the first estimate of the desired distribution. Projections are calculated from this distribution and arithmetically compared with the corresponding measured projections. This comparison may be a subtraction forming the basis for the algebraic techniques or a division that is characteristic of maximum likelihood algorithms. The result of this operation is backprojected to generate a correction image that is multiplied into the estimated distribution to complete the first iteration. This process is continued until the stopping criteria are met. Iterative algorithms are more time consuming than filtered backprojection, but they have several important advantages as follows:

1. They eliminate the radial streak artifacts, which accompany filtered backprojection.
2. They can effectively model and thereby correct for physical degradations of the imaging process such as scatter, attenuation, and spatial resolution.
3. They yield superior results in situations where a wide range of activities is present or where limited angle data is available.

These important advantages coupled with the increasing computational capabilities of computer systems now make iterative algorithms an attractive alternative.

IMAGE QUALITY

The ability to detect information in an image depends significantly on the signal-to-noise ratio (k). In the model developed by Rose, an estimate of the signal-to-noise ratio for white noise is given by:

$$k^2 = n\,C^2\,d^2 \tag{9}$$

where n is the image count density (counts/cm^2), C is the contrast between an area of interest and the surrounding region, and d is the linear dimension of the area. Although

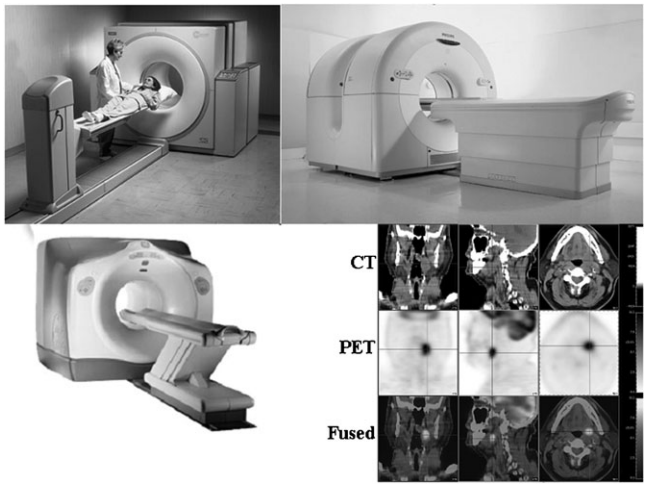

Figure 7. Commercial PET CT systems. These systems combine a fully functional CT scanner with a PET tomograph. The devices shown are the Siemens Biograph, Philips Gemini, and GE Discovery. The lower right image shows an example of the fused PET ^{18}F FDG and CT image data of a patient with lingual tonsilar carcinoma.

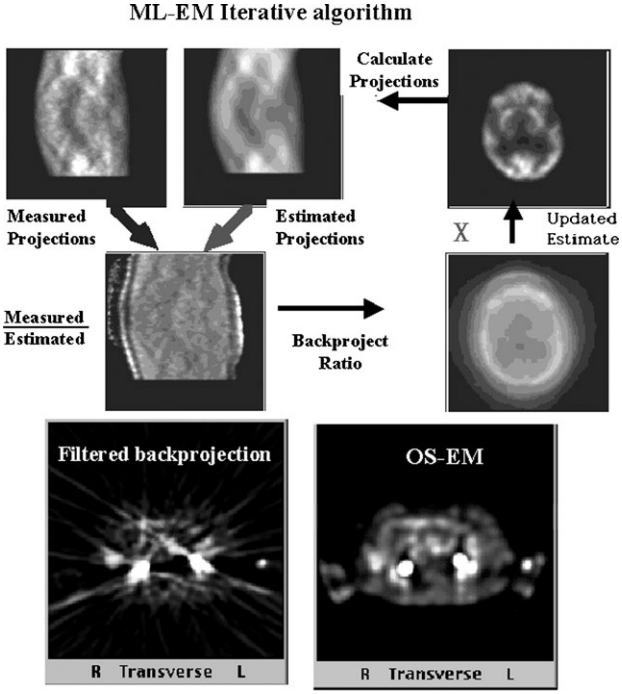

Figure 8. Iterative reconstruction. In iterative techniques, the calculated projections from the current estimate of the reconstructed image are arithmetically (difference or ratio) compared with the measured projection set. The result is backprojected and used to update the estimated reconstruction, which continues until the stopping criteria are reached. Maximum likelihood algorithms with rapid convergence such as the ordered subset approach are the most commonly used techniques. The images below show a comparison of an image reconstructed with filtered backprojection (left) and an ordered subset algorithm (8 subsets, 6 iterations). The iterative approach eliminates streak artifacts and yields a more accurate image in the vicinity of intense concentrations of activity.

this model is not strictly accurate for complicated image scenes or for cases where the noise is correlated as in tomography, it illustrates the importance of contrast and count density on detection. Although contrast primarily depends on the in vivo distribution of the radiotracer, the performance of the imaging system is an important factor especially for objects that are smaller than two $\times$ the FWHM associated with the system spatial resolution.

Spatial Resolution

The finite spatial resolution of radionuclide imaging reduces contrast, especially for small objects. Spatial resolution is characterized by the point or line spread response function (*PSF* or *LSF*). Although the entire response curve is needed to fully characterize the spatial resolution, often only the full-width-at-half-maximum is reported. The system spatial resolution depends on multiple components

including the intrinsic resolution of the detectors, the geometric resolution, and any spatial filtering. To the extent that each of these components have Gaussian response curves, the system FWHM (Rsys) is estimated from

$$R_{\text{sys}} = \left(\sum R_i\right)^{1/2} \tag{10}$$

where R_i is the FWHM associated with each component.

In SPECT imaging, the spatial resolution components are the intrinsic spatial resolution of the scintillation camera (typically 3.5 mm), the geometric resolution of the collimator (~8–15 mm depending on the source distance), and the kernel width of the windowed reconstruction filter (~5–15 mm depending on the count density). As the spatial resolution of the collimator depends on the source-to-collimator distance, it is important to maintain close proximity of the collimator to the patient whenever possible. All SPECT systems have body contouring capability for this reason.

In addition to the contribution from the reconstruction filter, four physical factors exist that limit the spatial resolution of PET systems: the size of the detector elements, the non-colinearity of the annihilation radiation, the positron range, and the detector parallax. Annihilation photons are co-linear only if the annihilation takes place with the positron and electron at rest. As thermal motion of the particles exists, about a 0.25° statistical deviation exists from true co-linearity. This deviation restricts the spatial resolution and becomes a larger problem as the coincidence detectors are separated at larger distances. Annihilation always takes place outside the nucleus after the positron has dissipated its energy. For low energy positrons such as emitted by ^{18}F, the reduction in spatial resolution from this effect is relatively small (<0.5 mm). However, for high energy positrons such as those emitted by ^{15}O, the contribution to spatial resolution is on the order of 1 mm. The thickness of the detectors becomes a limitation because interactions can happen at any depth within the crystal, which results in a position uncertainty for annihilation photons interacting obliquely with the thick crystals (30 mm) used in coincidence systems.

Image restoration techniques have been applied to SPECT and PET to partially compensate for losses due to spatial resolution. One approach uses restoration filters such as the Wiener or Metz filters, which combine a deconvolution of the point spread filter to restore resolution with a low pass filter to suppress noise amplification (17–21). These filters are usually used with filtered backprojection and been applied either to the projection data before reconstruction, or to the reconstructed images. Another approach restores spatial resolution by incorporating spatial resolution as a feature in iterative reconstruction (22).

Scatter

Compton scatter is the primary γ-ray interaction in body tissues. The energy of the Compton-scattered photons depends on the primary γ-ray energy and the scattering angle. As the energy resolution of scintillation detectors ranges from moderate [– 10% for 140-keV photons with NaI(Tl)] to poor (25% for 511-keV photons with BGO), scattered radiation cannot be totally eliminated with energy discrimination. For example, 140-keV photon scattered at a 50-degree angle would still be included in a 20% photopeak energy window. In a homogeneous medium, scattered radiation exhibits an exponential point spread response for both single photon and PET imaging systems. In non-homogeneous regions, the scatter response function becomes distorted because of the dependence of Compton scattering on tissue density.

Approximately 30–40% of the detected events in single photon imaging are due to scattered photons (23, 24). In 2-D PET, the fraction is less than 15%; but in 3-D PET, the fraction is on the order of 50%. Scattered radiation reduces image contrast in both PET and SPECT, and also may produce artifacts in myocardial perfusion studies that have been corrected for attenuation. Thus, it is desirable to reduce or eliminate scatter effects. One way to accomplish this effect is to use detectors with better energy resolution. The solid-state detector cadmium zinc telluride (CdZnTe) shows some promise as a potential replacement for NaI(Tl) (4). The substitution of LSO for BGO in PET imaging systems will significantly improve the energy resolution. The other alternative is to use processing techniques to reduce the scatter contribution. These techniques can be broadly grouped into subtraction-and model-based techniques. With the subtraction technique, one or more additional energy windows in the Compton energy range are acquired along with the primary photopeak data (25–28). With proper scaling, this information is directly subtracted from the photopeak data. Although this method is fast, it increases the noise level in the resulting images. Model-based techniques are usually incorporated as part of an iterative algorithm (29, 30). Scatter estimation is included as one of the physical processes in generating the current projection estimates. Accurate scatter modeling requires additional information about the density distribution in the patient, and it is time-intensive.

APPLICATIONS

Radionuclide imaging is used in a wide variety of diagnostic studies capable of evaluating the functional capacity of most of the organ systems. Radionuclide studies are routinely used to evaluate the brain, lungs, heart, liver, kidneys, GI tract, and the skeleton (Table 3). The most common SPECT study by far is myocardial perfusion for the noninvasive evaluation of coronary artery disease (Fig. 9).

In judging the performance of a diagnostic test for a specific disorder, two parameters are frequently used, sensitivity and specificity. The sensitivity of the test is the likelihood that the test is positive when disease is present:

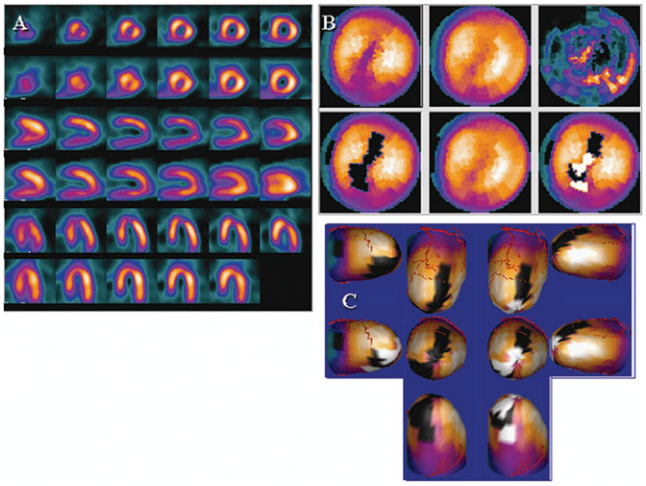

Figure 9. SPECT myocardial perfusion study. The radiotracers used in this study reflect the blood flow in the heart wall. Separate SPECT studies are acquired when the patient is in a normal resting state, and when the patient is subjected to a physical activity or a drug that requires more myocardial blood flow. Comparisons of these two studies indicate whether the patient is disease-free, has limited blood flow capacity (ischemia), or has permanent damage to the heart wall (infarct). (**a**) Tomographic stress and rest images of myocardial perfusion. The studies are often mapped to either circular (bulls-eye) or cylindrical (bullet) displays for easier viewing. (**b**) "Bulls-eye" display of myocardial perfusion. (**c**) "Bullet" display of the myocardial perfusion images.

$$\text{Sensitivity} = \text{True Positive Results/Actual Number of Positive Cases} \quad (11)$$

The specificity is the likelihood that the test is negative when that specific disease or disorder is not present:

$$\text{Specificity} = \text{True Negative Results/Actual Number of Nagative Cases} \quad (12)$$

Obviously, it is desirable to have both of these measures as close to 1.0 as possible. Many radionuclide studies do have both high sensitivity and high specificity, which along with the non-invasive feature makes them valuable diagnostic tools. However, a study that has only a high sensitivity or specificity can be valuable in the right setting for diagnosing a specific disorder. In this last section, a brief survey will be given on the use of radionuclide imaging in oncology.

Oncologic Imaging

The early and accurate diagnosis of cancer is extremely important. Many cancers can be cured or controlled if therapy is begun before the disease begins to spread from its local site of origin. Diagnostic studies are also important for monitoring therapy and for detecting recurrent disease. The ideal oncologic radiotracer would be taken up in high concentrations in malignant tissues with a long residence time and would clear rapidly from all others tissues. Unfortunately, there are no existing radiopharmaceuticals that are truly specific for cancer. All currently available cancer tracers distribute to some extent into normal tissues, some in quite high concentrations. Moreover, these tracers have varying levels of uptake in tumors based on tumor type and size as well as a variety of host factors.

A large number of radiopharmaceuticals have been used in oncologic imaging (31). ^{99m}Tc HDP, an agent that concentrates in the skeleton, is frequently used to detect metastatic disease in the bone. The bone scan is very sensitive for focal skeletal injury, but is non-specific for tumor as conditions like infection, trauma, and arthritis also result in altered tracer concentration (32). Another ^{99m}Tc tracer that concentrates in some tumors is sestamibi (33). Although ^{99m}Tc sestamibi is primarily used in the evaluation of myocardial perfusion, it is also useful in the detection of breast cancer, especially in dense breast tissue that cannot be reliably evaluated with mammography.

Radiolabeled monoclonal antibodies have shown some potential as diagnostic imaging agents (34–36). A monoclonal antibody is an immunologically active molecule designed to bind to a single antigen on tumor cells. If the antigen resides only on tumor cells, then the monoclonal antibody should bind specifically to the tumor. A number of radiolabeled antibodies have been investigated and several are currently available as diagnostic agents including ^{99m}Tc CEA Scan for colon cancer and ^{111}In ProstaScint (prostate cancer). Problems associated with radiolabeled antibodies include immunologic reactions, long clearance times resulting in high tissue background levels, and nonspecific binding to tissues other than the tumor. Some of the problems associated with radiolabeled monoclonal antibodies are avoided with radiolabeled peptides. Peptides are much smaller molecules than monoclonal antibodies and clear from the circulation much faster. In addition, they will not cause immunologic reactions. Indium-111 Pentetreotide, also referred to as Octreotide, is a peptide that binds to somatostatin receptors and is effective in imaging tumors that originate from neuro-endocrine tissues (Fig. 5)(37, 38).

The most successful tumor imaging agent today appears to be ^{18}F FDG (39, 40). The distribution of ^{18}F FDG depends

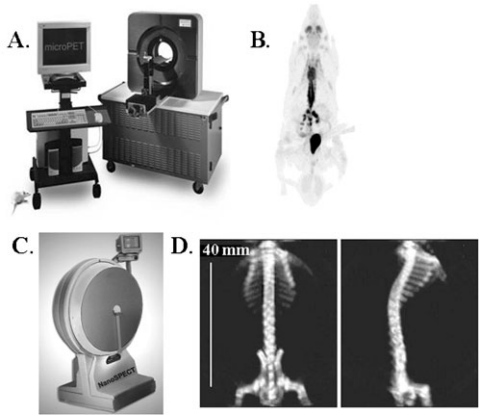

Figure 10. Small animal imaging systems. (**a**) Concorde MicroPET small animal PET system. (**b**) ^{18}F FDG whole body rat image. (**c**) Bioscan NanoSPECT small animal SPECT system. (**d**) Whole body ^{99m}Tc MDP bone scan of a mouse.

on glucose metabolic activity and most malignant tumors exhibit a much higher rate of glycolysis than most normal tissues, which makes ^{18}F FDG a very sensitive tumor agent (see Fig. 6). It should be noted that ^{18}F FDG uptake is not tumor-specific, and other conditions that cause glycolytic activity such as infection and post traumatic inflammation will also lead to increased uptake of ^{18}F FDG. Fluorine-18 FDG has very high sensitivity and specificity for lung, breast, head and neck, colon and pancreatic tumors, and also for malignant melanoma and lymphoma. By contrast, ^{18}F FDG has not performed well in detecting and staging prostatic cancer.

Small Animal Imaging Systems

The development of new radiopharmaceuticals and gene manipulation techniques requires the ability to perform radionuclide imaging on mice and rats. The imaging of these small animal presents challenges to PET and SPECT requiring large improvements in both spatial resolution and count sensitivity (41). These challenges have been at least partially met with new instrumentation that is now commercially available, which includes small animal PET systems with spatial resolution approaching 1 mm as well as small animal SPECT systems with sub-millimeter spatial resolution. The PET systems obtain this improvement in spatial resolution by reducing the detector size, whereas the SPECT systems rely on pinhole collimation. Although pinhole collimators have limited use for human imaging, they are very advantageous when the source distribution is localized in a limited region. Figure 10 shows examples of small animal PET and SPECT systems along with typical images.

SUMMARY

Radionuclide imaging provides a unique source of information about the physiology of tissues and organs. SPECT and PET imaging systems currently rely on scintillation detectors for acquiring projection information from the internally distributed radiotracers. Quantitative tomographic imaging requires correction for attenuation, scatter, and the finite spatial resolution of the imaging systems. Future developments will include improved detectors including semiconductors, faster and more sophisticated reconstruction algorithms, and better radiopharmaceuticals.

BIBLIOGRAPHY

1. Ice, R. D. History of Medical Radionuclide Production. *Health Physics* 1995, **69**(5),pp 721–727.
2. Votaw, J. R. The AAPM/RSNA Physics Tutorial for Residents. Physics of PET. *Radiographics* 1995, **15**(5), 1179-1190.
3. Wilkinson, F. In *Emission Tomography: The Fundamentals of SPECT and PET*; Wernick, M. N., Aarsvold, J. N., Eds., Elsevier: San Diego, CA, 2004, p 229–254.
4. Wagenaar, D. J. In *Emission Tomography: The Fundamentals of SPECT and PET*; Wernick, M. N., Aarsvold, J. N., Elsevier: San Diego, CA, 2004, pp 270–292.
5. Pichler, B. J., Ziegler, S. I. In *Emission Tomography: The Fundamentals of SPECT and PET*, Wernick, M. N., Aarsvold, J. N., Eds., Elsevier: San Diego, CA, 2004, pp 255–269.
6. Bailey, D. L., Meikle, S. R., Jones, T., Effective Sensitivity in 3D PET—The Impact of Detector Dead Time On 3D System Performance. *IEEE Trans. Nucl. Sci.* 1997, **44**(3 Part 2),pp 1180–1185.
7. Fahey, F. H. State of the Art in Emission Tomography Equipment. *Radiographics* 1996, **16**(2),pp 409–420.
8. King, M. A., Tsui, B. M., Pan, T. S. Attenuation Compensation for Cardiac Single-Photon Emission Computed Tomographic Imaging: Part 1. Impact of Attenuation and Methods of Estimating Attenuation Maps. *J. Nucl. Cardiol.* 1995, **2**(6),pp 513–524.
9. King, M. A., Tsui, B. M., Pan, T. S., Glick, S. J., Soares, E. J. Attenuation Compensation for Cardiac Single-Photon Emission Computed Tomographic Imaging: Part 2. Attenuation Compensation Algorithms. *J. Nucl. Cardiol.* 1996, **3**(1),pp 55–64.
10. O'Connor, M. K., Kemp, B. J. Single-Photon Emission Computed Tomography/Computed Tomography: Basic Instrumentation and Innovations. *Semin. Nucl. Med.* 2006, **36**(4),pp 258–266.
11. Vandenberghe, S., Daube-Witherspoon, M. E., Lewitt, R. M., Karp, J. S. Fast Reconstruction of 3D Time-of-Flight PET Data

by Axial Rebinning and Transverse Mashing. *Phys. Med. Biol.* 2006, **51**(6),pp 1603–1621.

12. Defrise, M., Kinahan, P. E., Townsend, D. W., Michel, C., Sibomana, M., Newport, D. F. Exact and Approximate Rebinning Algorithms for 3-D PET Data. *IEEE Trans. Med. Imaging.* 1997, **16**(2),pp 145–158.
13. Muehllehner, G., Karp, J. S. Positron Emission Tomography. *Phys. Med. Biol.* 2006, **51**(13),pp R117–R137.
14. Ell, P. J. PET/CT in Oncology: A Major Technology for Cancer Care. *Chang Gung Med. J.* 2005, **28**(5),pp 274–283.
15. Blodgett, T. M., Casagranda, B., Townsend, D. W., Meltzer, C. C. Issues, Controversies, and Clinical Utility of Combined PET/CT Imaging: What is the Interpreting Physician Facing? *AJR Am. J. Roentgenol.* 2005, **184**(5 Suppl),pp S138–S145.
16. Lalush, D. A., Wernick, M. N. In *Emission Tomography: The Fundamentals of SPECT and PET*; Wernick, M. N., Aarsvold, J. N. Elsevier: San Diego, CA, 2004, pp 44–472.
17. King, M. A., Doherty, P. W., Schwinger, R. B., Penney, B. C. A Wiener Filter for Nuclear Medicine Images. *Med. Phys.* 1983, **10**(6),pp 876–880.
18. King, M. A., Penney, B. C., Glick, S. J. An Image-Dependent Metz Filter for Nuclear Medicine Images. *J. Nucl. Med.* 1988, **29**(12) pp 1980–1989.
19. Links, J. M., Jeremy, R. W., Dyer, S. M., Frank, T. L., Becker, L. C. Wiener Filtering Improves Quantification of Regional Myocardial Perfusion with Thallium-201 SPECT. *J. Nucl. Med.* 1990, **31**(7),pp 1230–1236.
20. Madsen, M. T. A Method for Obtaining an Approximate Wiener Filter. *Med. Phys.* 1990, **17**(1),pp 126–130.
21. Miller, T. R., Sampathkumaran, K. S. Design and Application of Finite Impulse Response Digital Filters. *Euro. J. Nucl. Med.* 1982, **7**(1),pp 22–27.
22. Hutton, B. F., Lau, Y. H. Application of Distance-Dependent Resolution Compensation and Post-Reconstruction Filtering for Myocardial SPECT. *Phys. Med. Biol.* 1998, **43**(6),pp 1679–1693.
23. Rosenthal, M. S., Cullom, J., Hawkins, W., Moore, S. C., Tsui, B. M., Yester, M. Quantitative SPECT Imaging: A Review and Recommendations by the Focus Committee of the Society of Nuclear Medicine Computer and Instrumentation Council [see comments]. *J. Nucl. Med.* 1995, **36**(8),pp 1489–1513.
24. Tsui, B. M., Zhao, X., Frey, E. C., McCartney, W. H. Quantitative Single-Photon Emission Computed Tomography: Basics and Clinical Considerations. *Semin. Nucl. Med.* 1994, **24**(1),pp 38–65.
25. Buvat, I., Benali, H., Todd-Pokropek, A., Di Paola, R. Scatter Correction in Scintigraphy: The State of the Art. *Euro. J. Nucl. Med.* 1994, **21**(7),pp 675–694.
26. Buvat, I., Rodriguez-Villafuerte, M., Todd-Pokropek, A., Benali, H., Di Paola, R. Comparative Assessment of Nine Scatter Correction Methods Based on Spectral Analysis Using Monte Carlo Simulations. *J. Nucl. Med.* 1995, **36**(8),pp 1476–1488.
27. Ichihara, T., Ogawa, K., Motomura, N., Kubo, A., Hashimoto, S. Compton Scatter Compensation Using the Triple-Energy Window Method for Single- and Dual-Isotope SPECT. *J. Nucl. Med.* 1993, **34**(12),pp 2216–2221.
28. King, M. A., Hademenos, G. J., Glick, S. J. A Dual-Photopeak Window Method for Scatter Correction. *J. Nucl. Med.* 1992, **33**(4),pp 605–612.
29. Meikle, S. R., Hutton, B. F., Bailey, D. L. A Transmission-Dependent Method for Scatter Correction in SPECT. *J. Nucl. Med.* 1994, **35**(2),pp 360–367.
30. Welch, A., Gullberg, G. T., Christian, P. E., Datz, F. L., Morgan, H. T. A Transmission-Map-Based Scatter Correction Technique for SPECT in Inhomogeneous Media. *Med. Phys.* 1995, **22**(10),pp 1627–1635.
31. Abdel-Dayem, H. M. The Role of Nuclear Medicine in Primary Bone and Soft Tissue Tumors. *Semin. Nucl. Med.* 1997, **27**(4),pp 355–363.
32. Krasnow, A. Z., Hellman, R. S., Timins, M. E., Collier, B. D., Anderson, T., Isitman, A. T. Diagnostic Bone Scanning in Oncology. *Semin. Nucl. Med.* 1997, **27**(2),pp 107–141.
33. Waxman, A. D. The Role of (99m)Tc Methoxyisobutylisonitrile in Imaging Breast Cancer. *Semin. Nucl. Med.* 1997, **27**(1),pp 40–54.
34. Bischof Delaloye, A., Delaloye, B. Tumor Imaging with Monoclonal Antibodies. *Semin. Nucl. Med.* 1995, **25**(2),pp 144–164.
35. Nabi, H. A. Antibody Imaging in Breast Cancer. *Semin. Nucl. Med.* 1997, **27**(1),pp 30–39.
36. Zuckier, L. S., DeNardo, G. L. Trials and Tribulations: Oncological Antibody Imaging Comes to the Fore. *Semin. Nucl. Med.* 1997, **27**(1),pp 10–29.
37. de Herder, W. W., Kwekkeboom, D. J., Valkema, R., Feelders, R. A., van Aken, M. O., Lamberts, S. W., van der Lely, A. J., Krenning, E. P. Neuroendocrine Tumors and Somatostatin: Imaging Techniques. *J. Endocrinol. Invest.* 2005, **28**(11 Suppl),pp 132–136.
38. Teunissen, J. J., Kwekkeboom, D. J., Krenning, E. P. Staging and Treatment of Differentiated Thyroid Carcinoma with Radiolabeled Somatostatin Analogs. *Trends Endocrinol. Metab.* 2006, **17**(1),pp 19–25.
39. Hoh, C. K., Schiepers, C., Seltzer, M. A., Gambhir, S. S., Silverman, D. H., Czernin, J., Maddahi, J., Phelps, M. E. PET in Oncology: Will it Replace the Other Modalities? *Semin. Nucl. Med.* 1997, **27**(2),pp 94–106.
40. Langsteger, W., Heinisch, M., Fogelman, I. The Role of Fluorodeoxyglucose, 18F-Dihydroxyphenylalanine, 18F-Choline, and 18F-Fluoride in Bone Imaging with Emphasis on Prostate and Breast. *Semin. Nucl. Med.* 2006, **36**(1),pp 73–92.
41. Levin, C. S. Primer on Molecular Imaging Technology. *Eur. J. Nucl. Med. Mol. Imaging.* 2005, **32**(Suppl 2), pp S325–S345.

MARK T. MADSEN
University of Iowa, Iowa City, IA